https://doi.org/10.5194/egusphere-2026-5749
Preprint. Discussion started: 19 November 2026
© Author(s) 2026. CC BY 4.0 License.

Reanalyses may have limitations in representing the solar energy disposition of the Earth–atmosphere system

Guanghui Huang[1,2], Youjing Fu[1,2], Pengfei Zhao[1,2], Xudong Zheng[1,2], Shihong Zhang[1,2], Xiaohua Hao[3,4], Xufeng Wang[3,4]

[1]College of Earth and Environmental Sciences, Lanzhou University, Lanzhou 730000, China
[2]Center for Remote Sensing of Ecological Environments in Cold and Arid Regions, Lanzhou University, Lanzhou 730000, China
[3]Key Laboratory of Remote Sensing of Gansu Province, Northwest Institute of Eco-Environment and Resources, Chinese Academy of Sciences, Lanzhou 730000, China
[4]Heihe Remote Sensing Experimental Research Station, Northwest Institute of Eco-Environment and Resources, Chinese Academy of Sciences, Lanzhou 730000, China

Correspondence to: Youjing Fu (fuyj2025@lzu.edu.cn)

Abstract. Reanalysis data, including radiation data, are widely used in weather, climate, ecology, and water-cycle research. However, comprehensive evaluations of reanalysis solar energy disposition (SED) within the Earth–atmosphere system remain scarce. Combining collocated satellite and ground observations, this study evaluates the SED of three current representative reanalyses, ERA5 from ECMWF, CFSv2 from NCEP, and MERRA2 from NASA. The results demonstrate: 1) Among the three reanalyses, ERA5 exhibits the highest accuracy and most consistent performance across stations, while CFSv2 performs slightly better than MERRA2, which displays a pronounced systematic bias; 2) All three reanalyses demonstrate limited skill in representing the variability of atmospheric absorptance, explaining only a small fraction of the observed variance (the R^2 values of atmospheric absorptance between ERA5, CFSv2, and MERRA2 and observations are only 0.14, 0.12, and 0.14, respectively); 3) There appears to be a systematic bias in the three reanalyses, namely that atmospheric absorptance is substantially underestimated and surface absorptance is substantially overestimated, and this discrepancy is especially evident under overcast conditions. Our evaluations reveal that current reanalysis products may still have two inherent limitations in reproducing atmospheric absorptance, which may further affect the accuracies of the other two SED components.

1. Introduction

Solar radiation is the primary energy source driving Earth's dynamic, thermal, and hydrological processes (Huang et al., 2019). In global energy budget studies, the solar energy disposition (SED), comprising Top-of-Atmosphere (TOA) reflected radiation, atmosphere absorbing solar radiation, and surface absorbing solar radiation, provides a fundamental framework to quantify the distribution of solar energy and its associated feedback mechanisms (Li et al., 1997). TOA reflected radiation modulates the net solar energy input to the Earth–atmosphere system (Battisti and Donohoe, 2011), thereby strongly affecting the climate. Atmospheric solar absorption shapes vertical temperature gradients, turbulence, and convection (Li and Trishchenko, 2001), while surface solar absorption directly affects the surface energy balance and surface–atmosphere interactions (Yang et al., 2023). Accurate quantification of each

https://doi.org/10.5194/egusphere-2026-5749
Preprint. Discussion started: 19 November 2026
© Author(s) 2026. CC BY 4.0 License.

SED component is therefore essential for many related studies and applications (Wild and Bosilovich, 2024).

Reanalyses are generally produced by assimilating multisource in situ and satellite observations into numerical weather prediction models (Hersbach et al., 2020). Because they can provide long-term, temporally continuous, and spatially consistent fields of meteorological variables, reanalysis products have been widely used in a variety of geoscience studies (Zhang et al., 2020). Accordingly, radiation data given by reanalyses are also widely applied in studies, such as climate, ecology, and the water cycle. For example, in climate research, reanalysis-derived TOA radiation budgets are often used in the monitoring and analysis of global climate change (Trenberth et al., 2010; Trenberth et al., 2015). In terrestrial ecosystem studies, reanalysis-derived solar radiation and meteorological variables are widely used as forcing inputs for gross primary productivity (GPP) models to support global-scale carbon cycle analyses, as demonstrated by recent GPP datasets driven by ERA5 land climate fields (Wang et al., 2025). In hydrological applications, reanalysis radiative and atmospheric variables are commonly employed to estimate reference evapotranspiration and related water-cycle metrics at the global scale, supporting drought monitoring and food-security assessments (Hobbins et al., 2023).

Nevertheless, reanalysis radiation data still contain substantial uncertainties arising from model physical parameterizations, assimilated data quality, and simplifications in radiative transfer schemes. Early-generation reanalyses were found to systematically overestimate surface incident solar radiation (SSR), with global mean biases against site observations ranging widely from approximately 11 to 50 W m^{-2} (Zhang et al., 2016). Although the latest reanalyses, such as ERA5, show improved consistency in the climatology and seasonal variability of SSR, significant regional biases and long-term trend discrepancies remain (Jiao et al., 2022). Globally, reanalyses tend to overestimate the global mean SSR while underestimating surface incident longwave radiation by about 3–7 W m^{-2}, a deviation pattern also evident in climate models (Wild and Bosilovich, 2024). Given these repeated uncertainties and the existing validation efforts only on SSR, there is an urgent need for a comprehensive assessment of the reanalysis SED. Such an evaluation is essential for clearly identifying the limitations and characteristics of reanalysis products.

Thus, using collocated ground-based and satellite TOA observations, this study evaluates the SED components of three widely-used reanalysis products (ECMWF ERA5, NCEP CFSv2, and NASA MERRA2), and summarizes their limitations. The remainder of this paper is organized as follows: Sect. 2 describes the related physical variables and data; Sect. 3 presents the detailed evaluation results; current shortcomings of reanalysis SED are discussed in Sect. 4, followed by the conclusions in Sect. 5.

2. Physical variables and data

2.1. Variables describing the solar energy disposition

The incident solar radiation at the TOA is primarily governed by the solar zenith angles (SZA), which in turn strongly influence the absolute magnitudes of TOA reflected radiation, atmosphere absorbing solar radiation and surface absorbing solar radiation. To mitigate the influence of the SZA, this study employs planetary albedo (unit: %), atmospheric absorptance (unit: %), and surface absorptance (unit: %) to

https://doi.org/10.5194/egusphere-2026-5749
Preprint. Discussion started: 19 November 2026
© Author(s) 2026. CC BY 4.0 License.

characterize the three SED components. Being dimensionless, these variables can largely eliminate the site-specific dependencies in the evaluations and thereby enhance the generalization of our conclusions.

Planetary albedo (α_{plnt}) is defined as the percentage of the solar radiation reflected back to space by the atmosphere–surface system (including, e.g., clouds, aerosols, and the surface), to the TOA incident solar radiation (Battisti and Donohoe, 2011):

$$\alpha_{plnt} = 100 \times \frac{S^{\uparrow}_{TOA}}{S^{\downarrow}_{TOA}}\ \%, \tag{1}$$

where $S^{\downarrow}_{TOA}$ is the TOA incident solar radiation and $S^{\uparrow}_{TOA}$ is the TOA reflected radiation.

Surface absorptance (β_{surf}) is defined as the percentage of the solar radiation absorbed by the surface, to the TOA incident solar radiation:

$$\beta_{surf} = 100 \times \frac{S_{surf,net}}{S^{\downarrow}_{TOA}}\ \%, \tag{2}$$

where $S_{surf,net}$ is the net solar radiation absorbed at the surface, calculated as:

$$S_{surf,net} = S^{\downarrow}_{Surf} - S^{\uparrow}_{Surf} = \left(1 - \alpha_{surf}\right) S^{\downarrow}_{Surf}, \tag{3}$$

where $S^{\downarrow}_{Surf}$ and $S^{\uparrow}_{Surf}$ denote the downward and upward shortwave radiation at the surface, respectively. α_{surf} is the surface albedo.

Atmospheric absorptance (β_{atm}) is defined as the percentage of the solar radiation absorbed by atmospheric constituents (e.g., gases, aerosols, and clouds) to the TOA incident solar radiation:

$$\beta_{atm} = 100 \times \frac{S_{atm}}{S^{\downarrow}_{TOA}}\ \%. \tag{4}$$

Based on the principle of energy conservation, the energy absorbed by the atmosphere (S_{atm}) is derived from the net radiation balance between the TOA and the surface:

$$S_{atm} = (S^{\downarrow}_{TOA} - S^{\uparrow}_{TOA}) - S_{surf,net}. \tag{5}$$

Accordingly, these three dimensionless ratios satisfy the following closure relation:

$$\alpha_{plnt} + \beta_{atm} + \beta_{surf} = 1. \tag{6}$$

2.2. Reanalysis products

Three state-of-the-art global reanalysis products, ERA5, Climate Forecast System version 2 (CFSv2), and Modern-Era Retrospective Analysis for Research and Applications-2 (MERRA2), are evaluated in this study. ERA5 is the fifth-generation global atmospheric reanalysis (Hersbach et al., 2020) produced by the European Centre for Medium-Range Weather Forecasts (ECMWF), CFSv2 is the second version global atmospheric reanalysis (Saha et al., 2014) produced by the National Centers for Environmental Prediction (NCEP), whereas MERRA2 is the second version global atmospheric reanalysis produced by NASA's Global Modeling and Assimilation Office (Gelaro et al., 2017). These products represent the latest results of atmospheric reanalysis, which integrate the state-of-the-art global models and data assimilation systems.

The spatial resolution of ERA5 is 0.25° × 0.25° on a regular latitude–longitude grid. CFSv2 has a finer horizontal resolution of about 0.204° × 0.205° on an approximately regular latitude–longitude grid, and MERRA2 has a coarser resolution of about 0.5° × 0.625° on a non-uniform latitude–longitude grid. All

https://doi.org/10.5194/egusphere-2026-5749
Preprint. Discussion started: 19 November 2026
© Author(s) 2026. CC BY 4.0 License.

three reanalysis products provide the raw SED radiation fluxes at an hourly temporal resolution, from which the hourly SED variables (as defined in the previous section) can be derived directly.

2.3. Observational data and preprocessing

The observational data utilized by this study include TOA radiative flux products from the Clouds and the Earth's Radiant Energy System (CERES) aboard Terra and Aqua satellites, surface radiation measurements from three ground observing networks, and auxiliary cloud and albedo products provided by the Moderate Resolution Imaging Spectroradiometer (MODIS).

More specifically, CERES Single Scanner Footprint (SSF) products, which are derived from original radiance measurements using the Angular Distribution Model (Loeb et al., 2018), provide TOA flux observations at a 20-km resolution. SSF clear-sky fraction retrievals derived from collocated MODIS observations (Minnis et al., 2021) provide Fractional Cloud Cover (FCC) at a 20-km resolution. Surface radiative flux observations come from the Baseline Surface Radiation Network (BSRN), the Surface Radiation Budget Network (SURFRAD), and FLUXNET. BSRN and SURFRAD provide high-accuracy surface radiation measurements at 1-min resolution, with uncertainties typically below 2% (Augustine et al., 2000), whereas FLUXNET provides quality-controlled surface radiation measurements at 30-min resolution (Pastorello et al., 2020). Note that a station is selected for this study only if it has at least five consecutive years of observational data during 2012–2025, and the spatial distribution of final stations (total 80) is illustrated in Figure 1. Additionally, the MODIS MCD43A3 product at 500 m resolution provides the surface albedo data.

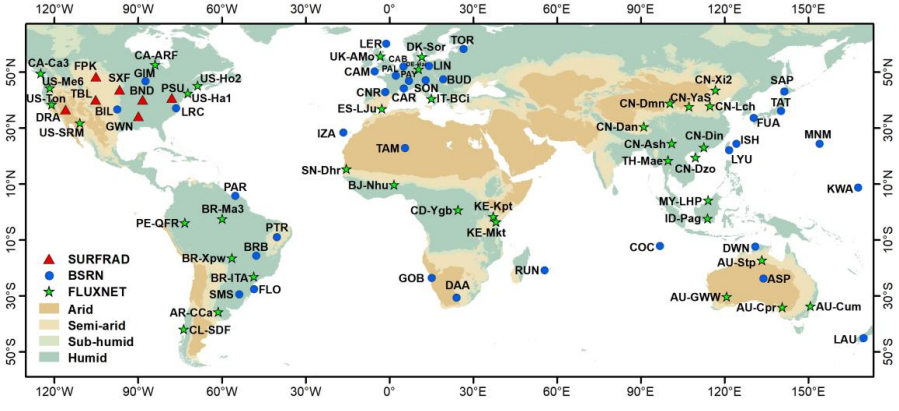
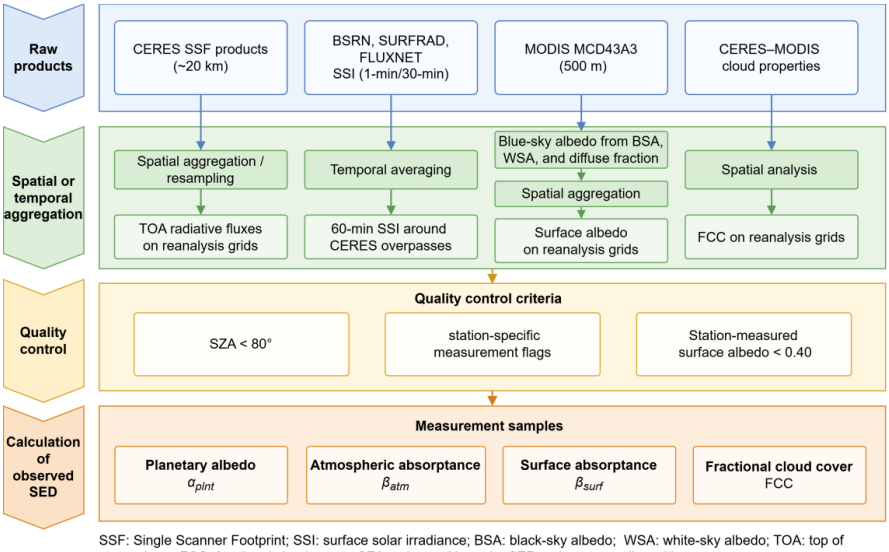


Figure 1. Global distribution of the 80 ground-based observation stations used in this study, with red triangles, blue circles, and green stars denoting SURFRAD, BSRN, and FLUXNET stations, respectively, and detailed station information provided in Appendix A, Table A1.

To ensure that observational data are rigorously matched in space and time with reanalysis products, a series of preprocessing steps are implemented as shown in Figure 2. First, given the coarse spatial resolution of reanalyses, CERES SSF TOA fluxes and fractional cloud cover are spatially aggregated or resampled into the grid scale of ERA5, CFSv2, or MERRA2. Next, high-frequency surface incident solar radiation measurements from BSRN, SURFRAD and FLUXNET are averaged into hourly means using a ±30 min window, to enhance the spatial representativeness of the station observations (Huang et al.,

https://doi.org/10.5194/egusphere-2026-5749
Preprint. Discussion started: 19 November 2026
© Author(s) 2026. CC BY 4.0 License.

2016; Jiang et al., 2020). Then, to account for the strong spatial heterogeneity of surface reflected radiation, the MODIS albedo product MCD43A3 is introduced, and the albedo and surface absorptance matching the resolution of the reanalysis products are recalculated. Furthermore, to reduce the impact of snow cover, samples with anomalously high surface albedo are excluded. Finally, three observational datasets are prepared, each matched to the spatial resolution of ERA5, CFSv2, or MERRA2.



SSF: Single Scanner Footprint; SSI: surface solar irradiance; BSA: black-sky albedo; WSA: white-sky albedo; TOA: top of atmosphere; FCC: fractional cloud cover; SZA: solar zenith angle; SED: solar energy disposition.

Figure 2. Preprocessing workflow for deriving observational SED components at reanalysis-specific spatial scales.

3. Results

The SED in ERA5, CFSv2, and MERRA2 is evaluated using quality-controlled, spatiotemporally collocated satellite and ground-based observations at 80 stations during 2012–2025. Because atmospheric moisture, cloud conditions, and surface characteristics influence how solar energy is reflected and absorbed, the accuracy with which reanalyses represent SED may vary across hydroclimatic conditions. To examine this possibility, the stations were grouped into four classes based on the annual Global Aridity Index v3 climatology (Zomer et al., 2022): arid (namely hyper-arid and arid classes in their paper), semi-arid, sub-humid (namely dry sub-humid class in their paper), and humid.

3.1. Evaluation of ECMWF ERA5 SED

The overall evaluation of ECMWF ERA5 SED is conducted across all stations, and the detailed statistics are listed in Table 1. ERA5 shows a near-zero bias (0.04%) for planetary albedo, a modest negative bias (−1.58%) for atmospheric absorptance, and a corresponding modest positive bias (1.54%) for surface absorptance. The mean absolute errors (MAEs) are 6.45%, 6.22%, and 9.65%, and the root mean square errors (RMSEs) are 9.46%, 8.86%, and 13.44%, respectively. Surface absorptance has the largest MAE and RMSE but the lowest relative RMSE (28.40%), which may be due to its larger reference value.

https://doi.org/10.5194/egusphere-2026-5749
Preprint. Discussion started: 19 November 2026
© Author(s) 2026. CC BY 4.0 License.

Atmospheric absorptance shows the weakest agreement with observations, with an R^2 value of 0.14, compared with 0.63 for planetary albedo and 0.54 for surface absorptance. Overall, ERA5 represents planetary albedo well in terms of mean bias and agreement with observations.

The statistics for the four aridity classes reveal broadly consistent patterns among the three SED components. For planetary albedo, RMSE increases across the four classes, from 7.08% at arid stations to 10.19% at humid stations. For atmospheric absorptance, RMSE is higher in the semi-arid (9.54%) and humid (9.36%) classes than in the arid (6.52%) and sub-humid (7.15%) classes. The atmospheric absorptance bias is also more negative at humid stations (−2.09%) than at arid stations (−0.66%). For surface absorptance, RMSE is lowest in the arid class (9.97%) and highest in the humid class (14.27%). Its relative RMSE increases across the four aridity classes, from 18.33% at arid stations to 32.96% at humid stations.

Table 1. Statistics of ECMWF ERA5 SED validation across all stations.

Aridity class	Variables	Obs. Mean (%)	Bias (%)	MAE (%)	RMSE (%)	Relative RMSE (%)	R^2
All	Planetary albedo	28.61	0.04	6.45	9.46	33.06	0.63
	Atmospheric absorptance	24.05	−1.58	6.22	8.86	36.86	0.14
	Surface absorptance	47.34	1.54	9.65	13.44	28.40	0.54
Arid	Planetary albedo	24.18	0.31	4.24	7.08	29.27	0.52
	Atmospheric absorptance	21.40	−0.66	4.54	6.52	30.46	0.22
	Surface absorptance	54.43	0.36	6.71	9.97	18.33	0.50
Semi-arid	Planetary albedo	24.31	−0.34	5.29	8.29	34.12	0.57
	Atmospheric absorptance	21.93	−1.12	6.58	9.54	43.49	0.12
	Surface absorptance	53.76	1.46	9.26	13.23	24.61	0.44
Sub-humid	Planetary albedo	27.42	0.63	6.76	9.87	35.98	0.62
	Atmospheric absorptance	22.87	−0.58	4.99	7.15	31.27	0.12
	Surface absorptance	49.71	−0.06	9.17	12.94	26.04	0.55
Humid	Planetary albedo	31.18	−0.01	7.27	10.19	32.70	0.63
	Atmospheric absorptance	25.52	−2.09	6.70	9.36	36.68	0.09
	Surface absorptance	43.30	2.10	10.54	14.27	32.96	0.53

Figure 3 presents the station-specific error distributions. Across all three SED components, arid stations generally have smaller interquartile ranges, whereas larger interquartile ranges and longer whiskers occur at many semi-arid, sub-humid, and humid stations. For planetary albedo, most boxplots are centered near zero, with no consistent error direction across the four aridity groups. Both atmospheric absorptance underestimation and surface absorptance overestimation are most common among humid stations. At the station-mean level, atmospheric absorptance underestimation accompanied by surface absorptance overestimation occurs at 3 of 9 arid stations, 7 of 15 semi-arid stations, 2 of 7 sub-humid stations, and 36 of 49 humid stations.

The humid stations AR-CCa, LYU, and MY-LHP and the semi-arid station ES-LJu illustrate this combination: atmospheric absorptance errors are strongly negative, surface absorptance errors are positive, and planetary albedo errors are comparatively small. In contrast, atmospheric absorptance errors are positive at the semi-arid stations IZA and CN-Xi2 and the arid station TAM; IZA and TAM also show negative surface absorptance errors. IZA is a high-mountain station representative of the subtropical North Atlantic free troposphere (García et al., 2019), which may partly explain its distinct error characteristics. Overall, the station-level results are consistent with the near-zero mean planetary

https://doi.org/10.5194/egusphere-2026-5749
Preprint. Discussion started: 19 November 2026
© Author(s) 2026. CC BY 4.0 License.

albedo bias reported in Table 1 and show that atmospheric absorptance underestimation and surface absorptance overestimation are particularly common at humid stations.

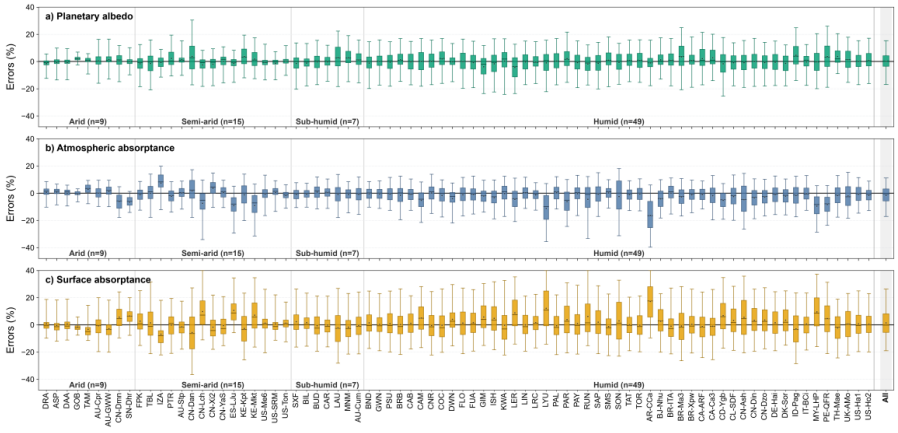


Figure 3. Station-specific distributions of SED errors for ECMWF ERA5: a) planetary albedo, b) atmospheric absorptance, and c) surface absorptance; boxes show the interquartile range, center lines show medians, dots show means, and whiskers indicate the 5th and 95th percentiles; stations are grouped by arid, semi-arid, sub-humid, and humid classes; the "All" column combines samples from all 80 stations.

3.2. Evaluation of NCEP CFSv2 SED

Table 2 presents the overall evaluation statistics for NCEP CFSv2 SED. CFSv2 exhibits negative biases for planetary albedo (−0.67%) and atmospheric absorptance (−2.42%), together with a positive bias for surface absorptance (3.09%). Both absorptance biases are larger in magnitude than those in ERA5. The MAEs are 9.25%, 6.35%, and 12.02%, and the RMSEs are 13.46%, 9.10%, and 17.07%, respectively. As in ERA5, surface absorptance has the largest MAE and RMSE, while atmospheric absorptance has the lowest R^2 value (0.12), compared with 0.47 for planetary albedo and 0.42 for surface absorptance.

The statistics for the four aridity classes also show patterns similar to those in ERA5. For planetary albedo, RMSE increases across the four classes, from 10.98% at arid stations to 14.42% at humid stations. For atmospheric absorptance, RMSE is higher in the semi-arid (9.65%) and humid (9.64%) classes than in the arid (6.82%) and sub-humid (7.27%) classes. The atmospheric absorptance bias is most negative in the humid class (−2.96%). For surface absorptance, RMSE is lowest in the arid class (13.98%) and highest in the humid class (18.03%). Its relative RMSE increases across the four classes, from 25.72% at arid stations to 41.73% at humid stations.

Table 2. Statistics of NCEP CFSv2 SED validation across all stations.

Aridity class	Variables	Obs. Mean (%)	Bias (%)	MAE (%)	RMSE (%)	Relative RMSE (%)	R^2
All	Planetary albedo	28.69	−0.67	9.25	13.46	46.91	0.47
	Atmospheric absorptance	24.03	−2.42	6.35	9.10	37.87	0.12
	Surface absorptance	47.28	3.09	12.02	17.07	36.11	0.42
Arid	Planetary albedo	24.20	0.06	7.14	10.98	45.38	0.28
	Atmospheric absorptance	21.46	−1.50	4.85	6.82	31.79	0.16

https://doi.org/10.5194/egusphere-2026-5749
Preprint. Discussion started: 19 November 2026
© Author(s) 2026. CC BY 4.0 License.

	Surface absorptance	54.33	1.44	9.92	13.98	25.72	0.26
Semi-arid	Planetary albedo	24.43	−0.28	7.67	11.99	49.08	0.41
	Atmospheric absorptance	21.79	−1.91	6.60	9.65	44.31	0.12
	Surface absorptance	53.79	2.19	11.02	16.53	30.74	0.32
Sub-humid	Planetary albedo	27.53	−1.58	8.80	13.25	48.12	0.47
	Atmospheric absorptance	22.93	−1.41	4.97	7.27	31.71	0.11
	Surface absorptance	49.54	2.99	10.70	16.05	32.40	0.44
Humid	Planetary albedo	31.27	−0.81	10.32	14.42	46.12	0.49
	Atmospheric absorptance	25.52	−2.96	6.85	9.64	37.77	0.07
	Surface absorptance	43.21	3.77	13.04	18.03	41.73	0.43

Figure 4 presents the station-specific CFSv2 error distributions across the four aridity groups. As in ERA5, arid stations generally have smaller interquartile ranges, whereas larger interquartile ranges and longer whiskers occur at many semi-arid, sub-humid, and humid stations. For planetary albedo, negative station-mean errors are more common, particularly in the sub-humid and humid groups. For atmospheric absorptance, station-mean errors are predominantly negative in the semi-arid, sub-humid, and humid groups. For surface absorptance, both positive and negative station-mean errors occur in the arid and semi-arid groups, whereas positive errors predominate in the sub-humid and humid groups. At the station-mean level, atmospheric absorptance underestimation accompanied by surface absorptance overestimation occurs at 4 of the 9 arid stations, 9 of the 15 semi-arid stations, 6 of the 7 sub-humid stations, and 38 of the 49 humid stations.

The humid stations AR-CCa, LYU, and MY-LHP and the semi-arid station KE-Mkt exhibit pronounced atmospheric absorptance underestimation accompanied by surface absorptance overestimation. Conversely, positive atmospheric absorptance errors occur at the semi-arid station IZA and the arid station TAM, together with negative surface absorptance errors. Overall, both CFSv2 and ERA5 generally underestimate atmospheric absorptance and overestimate surface absorptance, but CFSv2 shows broader station-level error distributions for planetary albedo and surface absorptance.

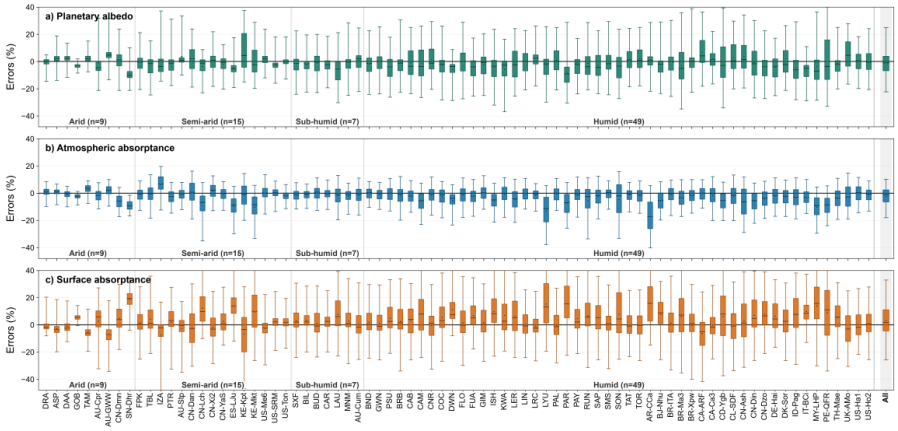


Figure 4. Station-specific distributions of SED errors for NCEP CFSv2: a) planetary albedo, b) atmospheric absorptance, and c) surface absorptance; boxes show the interquartile range, center lines show medians, and dots show means, and whiskers indicate the 5th and 95th percentiles; stations are grouped

https://doi.org/10.5194/egusphere-2026-5749
Preprint. Discussion started: 19 November 2026
© Author(s) 2026. CC BY 4.0 License.

by arid, semi-arid, sub-humid, and humid classes; the "All" column combines samples from all 80 stations.

3.3. Evaluation of NASA MERRA2 SED

Table 3 summarizes the overall evaluation statistics for NASA MERRA2 SED. MERRA2 exhibits negative biases for planetary albedo (−1.05%) and atmospheric absorptance (−4.28%), together with a positive bias for surface absorptance (5.33%). The biases in all three components are larger in magnitude than the corresponding biases in ERA5 and CFSv2. The MAEs are 7.44%, 7.07%, and 11.07%, and the RMSEs are 10.89%, 9.99%, and 15.64%, respectively. As in ERA5 and CFSv2, surface absorptance has the largest MAE and RMSE, while atmospheric absorptance has the lowest R^2 value (0.14), compared with 0.51 for planetary albedo and 0.45 for surface absorptance.

Across the four aridity classes, planetary albedo RMSE increases from 7.60% at arid stations to 11.98% at humid stations. For atmospheric absorptance, RMSE is higher in the semi-arid (10.31%) and humid (10.68%) classes than in the arid (7.28%) and sub-humid (8.06%) classes. Its bias is most negative at humid stations (−5.09%), compared with −2.66% at arid stations. For surface absorptance, RMSE increases across the four classes, from 10.88% at arid stations to 16.98% at humid stations. Its relative RMSE also increases across the four classes, from 19.85% to 38.94%, while its positive bias is greater at humid stations (6.41%) than at arid stations (2.35%).

Table 3. Statistics of NASA MERRA2 SED validation across all stations.

Aridity class	Variables	Obs. Mean (%)	Bias (%)	MAE (%)	RMSE (%)	Relative RMSE (%)	R^2
All	Planetary albedo	28.14	−1.05	7.44	10.89	38.68	0.51
	Atmospheric absorptance	24.22	−4.28	7.07	9.99	41.26	0.14
	Surface absorptance	47.64	5.33	11.07	15.64	32.84	0.45
Arid	Planetary albedo	24.06	0.31	4.56	7.60	31.57	0.45
	Atmospheric absorptance	21.12	−2.66	4.98	7.28	34.45	0.21
	Surface absorptance	54.83	2.35	7.06	10.88	19.85	0.44
Semi-arid	Planetary albedo	23.55	−1.22	5.76	8.92	37.87	0.51
	Atmospheric absorptance	22.27	−3.50	7.03	10.31	46.29	0.12
	Surface absorptance	54.17	4.71	9.81	14.45	26.67	0.40
Sub-humid	Planetary albedo	26.69	−1.01	7.45	11.10	41.60	0.50
	Atmospheric absorptance	22.85	−2.97	5.63	8.06	35.28	0.11
	Surface absorptance	50.45	3.97	10.19	14.89	29.52	0.45
Humid	Planetary albedo	30.68	−1.32	8.61	11.98	39.04	0.50
	Atmospheric absorptance	25.72	−5.09	7.79	10.68	41.54	0.09
	Surface absorptance	43.60	6.41	12.51	16.98	38.94	0.42

Figure 5 presents the station-specific MERRA2 error distributions across the four aridity groups. As in ERA5 and CFSv2, arid stations generally have smaller interquartile ranges, whereas larger interquartile ranges and longer whiskers occur at many semi-arid, sub-humid, and humid stations. For planetary albedo, approximately two-thirds of the stations have negative mean errors. For atmospheric absorptance, station-mean errors are predominantly negative in all four groups. For surface absorptance, station-mean errors are predominantly positive in all four groups. At the station-mean level, atmospheric absorptance underestimation accompanied by surface absorptance overestimation occurs at 6 of the 9

https://doi.org/10.5194/egusphere-2026-5749
Preprint. Discussion started: 19 November 2026
© Author(s) 2026. CC BY 4.0 License.

arid stations, 14 of the 15 semi-arid stations, 6 of the 7 sub-humid stations, and 45 of the 49 humid stations.

Representative examples include the humid stations AR-CCa and LYU and the semi-arid stations ES-LJu and KE-Mkt, where pronounced negative atmospheric absorptance errors are accompanied by positive surface absorptance errors. Positive atmospheric absorptance errors occur at only four stations: the semi-arid station IZA, the arid stations TAM and DRA, and the humid station SON. At IZA and TAM, positive atmospheric absorptance errors are accompanied by negative surface absorptance errors, as also observed for ERA5 and CFSv2. Overall, the combination of atmospheric absorptance underestimation and surface absorptance overestimation occurs at more stations in MERRA2 than in ERA5 or CFSv2.

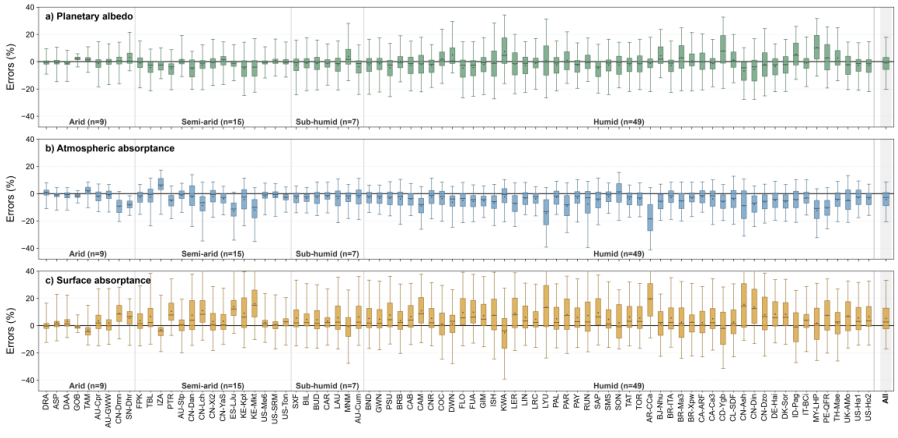


Figure 5. Station-specific distributions of SED errors for NASA MERRA2: a) planetary albedo, b) atmospheric absorptance, and c) surface absorptance; boxes show the interquartile range, center lines show medians, dots show means, and whiskers indicate the 5th and 95th percentiles; stations are grouped by arid, semi-arid, sub-humid, and humid classes; the "All" column combines samples from all 80 stations.

Comparison of Tables 1–3 and Figs. 3–5 shows that ERA5 has the smallest overall errors. CFSv2 has broader station-level error distributions than ERA5 for planetary albedo and surface absorptance, whereas MERRA2 has the largest biases in magnitude for all three components. Across all three products and SED components, station-level error distributions are generally narrower at arid stations and broader at humid stations. The combination of atmospheric absorptance underestimation and surface absorptance overestimation is concentrated in the humid group for ERA5, occurs at most of the semi-arid, sub-humid, and humid stations for CFSv2, and predominates across all four groups for MERRA2. Overall, MERRA2 shows the most widespread systematic deviations in atmospheric and surface absorptance.

https://doi.org/10.5194/egusphere-2026-5749
Preprint. Discussion started: 19 November 2026
© Author(s) 2026. CC BY 4.0 License.

4. Discussions

4.1. Intercomparison of reanalysis SED performances

The above evaluations of the three reanalysis products indicate that ECMWF ERA5 generally outperforms NCEP CFSv2 and NASA MERRA2 in representing the solar energy disposition of the Earth–atmosphere system. A comparison of Tables 1–3 shows that ERA5 has the smallest RMSEs for all three SED components and the highest R^2 values for planetary albedo and surface absorptance. The R^2 values for atmospheric absorptance are similarly low in all three reanalyses. Comparing Table 2 with Table 3 further shows that each product has distinct strengths. CFSv2 has smaller biases in all three components and a smaller RMSE for atmospheric absorptance, whereas MERRA2 has smaller RMSEs for planetary albedo and surface absorptance. The major issue for MERRA2 is its pronounced systematic deviations.

The intercomparison of Figs. 3–5 further shows that ERA5 combines higher overall accuracy with generally more compact station-level error distributions. CFSv2 exhibits broader distributions and greater differences among stations, particularly for planetary albedo and surface absorptance. MERRA2, in contrast, shows more consistent error directions, with planetary albedo and atmospheric absorptance underestimated at most stations and surface absorptance predominantly overestimated. The concurrent underestimation of atmospheric absorptance and overestimation of surface absorptance is concentrated among humid stations in ERA5, occurs at most of the semi-arid, sub-humid, and humid stations in CFSv2, and is widespread across all four aridity groups in MERRA2. Reanalysis performance also differs among the four aridity classes. Across all three products, planetary albedo and surface absorptance errors are generally smaller in the arid group and larger in the humid group. Atmospheric absorptance errors tend to be larger in the semi-arid and humid groups than in the arid and sub-humid groups.

4.2. Accuracies of reanalysis fractional cloud cover

Fractional cloud cover directly affects the solar energy partitioning in the Earth–atmosphere system and is therefore a key factor influencing the accuracy of reanalysis SED. In this section, we accordingly evaluate the fractional cloud cover accuracy (unit: %) of the three reanalysis products.

Figure 6 presents the probability density functions of fractional cloud cover errors for ERA5 (green), CFSv2 (blue), and MERRA2 (orange). Note that the observed fractional cloud cover used here is obtained from the CERES–MODIS cloud products, which are derived from collocated MODIS imager observations and spatially matched to the grid of each reanalysis. As shown in the figure, the majority of fractional cloud cover errors fall within ±20% (69.49% for ERA5, 62.17% for CFSv2, and 54.02% for MERRA2). The error probability peaks for ERA5 and CFSv2 are both near zero, whereas that for MERRA2 is clearly below zero. Relative to observations, ERA5 shows a negative bias of −1.93%, CFSv2 exhibits a larger negative bias of −3.45%, and MERRA2 displays a substantial negative bias of −10.50%. The corresponding mean absolute errors (MAEs) are 16.09%, 21.93%, and 25.35%, and the R^2 values are 0.63, 0.43, and 0.37, respectively. ERA5 maintains the best performance, followed by CFSv2, while MERRA2 considerably underestimates fractional cloud cover.

Given that clouds are perhaps the largest uncertainty in climate models (Norris et al., 2016), the fractional cloud cover accuracy achieved by these reanalyses is somewhat surprising. In the previous

https://doi.org/10.5194/egusphere-2026-5749
Preprint. Discussion started: 19 November 2026
© Author(s) 2026. CC BY 4.0 License.

evaluations, the all-sky evaluations in fact encompass extreme cases where the atmospheric conditions simulated by reanalyses are completely opposite to those observed. In Fig. 6, such extreme cases fall into the error ranges of −100% to −90% and 90% to 100%, accounting for approximately 0.41% of the ERA5 samples, 2.83% of the CFSv2 samples, and 1.37% of the MERRA2 samples. These cloud-condition mismatches are retained in the all-sky evaluation, whereas Sect. 4.4 further examines samples for which CERES and the corresponding reanalysis indicate the same sky condition.

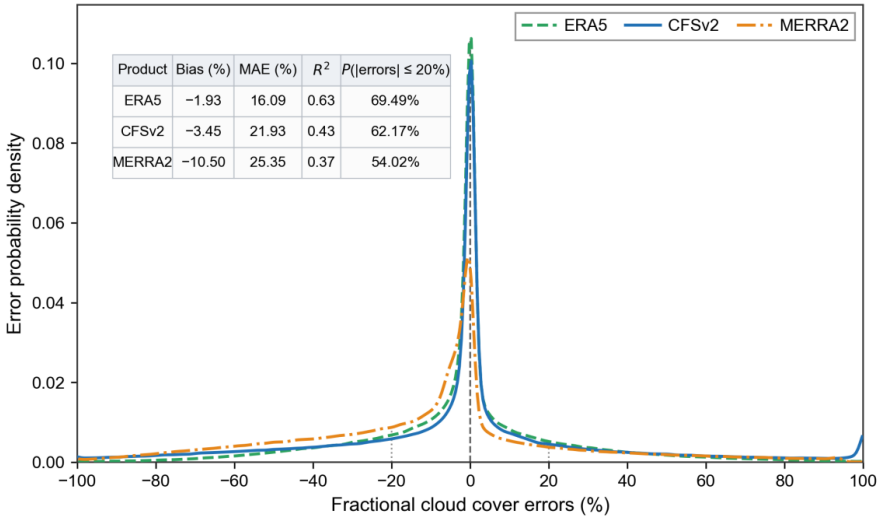


Figure 6. Distributions of fractional cloud cover errors in three reanalysis products: ECMWF ERA5 (green), NCEP CFSv2 (blue), and NASA MERRA2 (orange).

4.3. Limited representation of atmospheric absorptance variability

In the preceding evaluations, we note that the correlations between atmospheric absorptance from the three reanalysis products and observations are consistently low. Under instantaneous all-sky conditions, the R^2 values are only 0.14 for ERA5, 0.12 for CFSv2, and 0.14 for MERRA2. These results suggest that the reanalysis products have limited ability to represent the variability of atmospheric absorptance.

Figure 7 provides a more direct comparison between the reanalyses and observations under instantaneous all-sky conditions. The standard deviations of atmospheric absorptance from the observations are 9.38%, 9.34%, and 9.66% for the ERA5, CFSv2, and MERRA2 matched samples, respectively. In comparison, the corresponding standard deviations from the reanalyses are substantially lower, at 3.04%, 3.23%, and 2.59%. Thus, the reanalysis standard deviations are only 27%–35% of those from the observations. The density plots also show that atmospheric absorptance from the reanalyses is concentrated within a much narrower range than that from the observations. Therefore, all three reanalyses demonstrate limited capability in representing the variability of atmospheric absorptance.

https://doi.org/10.5194/egusphere-2026-5749
Preprint. Discussion started: 19 November 2026
© Author(s) 2026. CC BY 4.0 License.

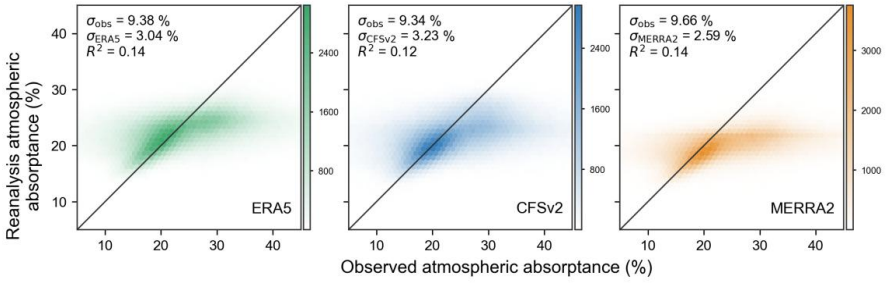


Figure 7. Comparison of instantaneous atmospheric absorptance between reanalysis products and observations under all-sky conditions.

To check whether this discrepancy disappears or is mitigated at longer timescales, we also compare daily and monthly atmospheric absorptance derived from valid matched daylight hours, as shown in Fig. 8. At the daily scale, the R^2 values increase modestly to 0.18, 0.16, and 0.19 for ERA5, CFSv2, and MERRA2, respectively. However, the reanalysis standard deviations remain substantially lower, ranging from 2.36% to 2.72%, compared with approximately 7.40% in the observations. At the monthly scale, the R^2 values increase to 0.26, 0.21, and 0.30, while the standard deviations remain only 1.78%–2.11% in the reanalyses compared with 4.86% in the observations. It should be noted, however, that differences between the instantaneous and longer-timescale results cannot be attributed solely to temporal aggregation, because the daily and monthly evaluations use CERES SYN1deg data on a common 1° grid. Nevertheless, the substantially narrower range of atmospheric absorptance remains evident at all three evaluation scales.

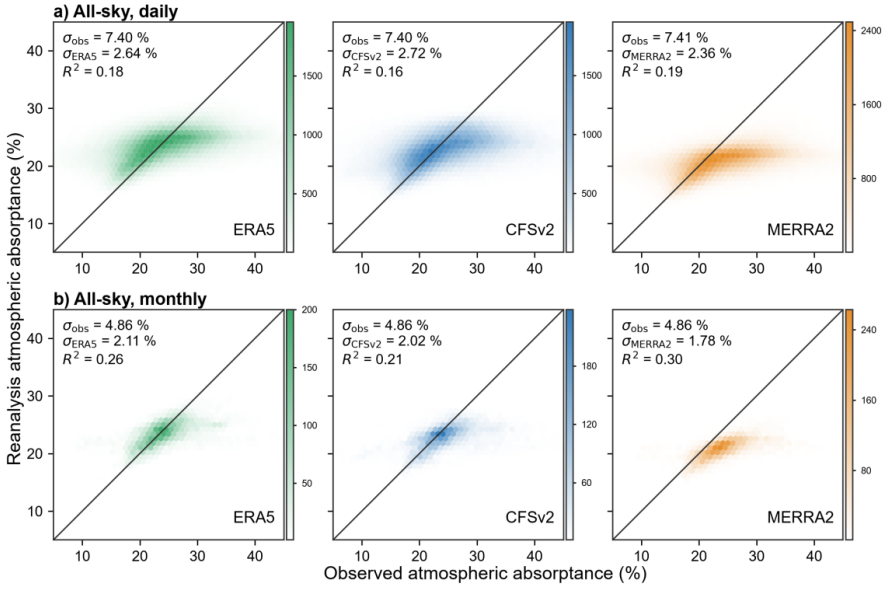


Figure 8. Comparison of atmospheric absorptance between reanalysis products and observations under all-sky conditions at a) daily and b) monthly timescales, based on daylight-hour data.

https://doi.org/10.5194/egusphere-2026-5749
Preprint. Discussion started: 19 November 2026
© Author(s) 2026. CC BY 4.0 License.

4.4. Systematic bias of reanalysis SED

In Sect. 3, we have noted that reanalysis SED may exhibit systematic deviations. Under all-sky conditions, all three reanalyses exhibit a negative bias in atmospheric absorptance and a positive bias in surface absorptance. Figure 9 further examines these deviations under three sky conditions defined by fractional cloud cover (FCC): clear (0% ⩽ FCC ⩽ 5%), partly cloudy (5% < FCC < 95%), and overcast (95% ⩽ FCC ⩽ 100%) (American Meteorological Society, 2026). To exclude cases in which the observed and reanalysis sky conditions differ, Figure 9 includes only samples for which CERES and the corresponding reanalysis identify the same sky condition: clear, partly cloudy, or overcast.

Under clear-sky conditions, the biases of all three SED components remain within ±1% in ERA5 and CFSv2, whereas MERRA2 shows biases of −1.72% and 1.49% in atmospheric and surface absorptance, respectively. The atmospheric absorptance biases under partly cloudy conditions are −1.25%, −2.67%, and −3.85% for ERA5, CFSv2, and MERRA2, respectively, and become −2.68%, −2.45%, and −6.08% under overcast conditions. Thus, atmospheric absorptance underestimation generally becomes more pronounced under cloudy conditions, particularly in MERRA2. Under overcast conditions, ERA5 also shows biases of −1.87% and 4.55% in planetary albedo and surface absorptance, respectively. In CFSv2 and MERRA2, the negative atmospheric absorptance biases are accompanied by positive biases in planetary albedo and surface absorptance, which are 2.05% and 0.40% for CFSv2 and 2.51% and 3.57% for MERRA2, respectively.

The station-level patterns under matched sky conditions further demonstrate how cloud cover modifies the spatial prevalence of these systematic biases. Relative to the all-sky results reported in Sect. 3, atmospheric absorptance underestimation becomes more widespread under overcast conditions, occurring at 76, 75, and 79 of the 80 stations for ERA5, CFSv2, and MERRA2, respectively. Surface absorptance is overestimated at 77, 47, and 64 stations under overcast conditions. The particularly high frequency in ERA5 indicates that its atmospheric absorptance underestimation is compensated predominantly by surface absorptance overestimation. In CFSv2 and MERRA2, the smaller number of stations with positive surface absorptance biases is consistent with the additional compensating contribution from planetary albedo. Overall, atmospheric absorptance underestimation is the most consistent systematic deviation across the three products and occurs at more stations under overcast conditions. Systematic deviations of solar energy disposition in models, particularly the underestimation of atmospheric absorptance, have long been a subject of great controversy (Li and Moreau, 1996; Fu et al., 2026). Since both ERA5 and MERRA2 incorporate MODIS albedo products as model input (Gelaro et al., 2017; Hersbach et al., 2020), this suggests a likely overestimation of surface incident radiation. Such an error feature is consistent with the previous evaluations for these reanalysis products (Zhang et al., 2016; Wild and Bosilovich, 2024).

https://doi.org/10.5194/egusphere-2026-5749
Preprint. Discussion started: 19 November 2026
© Author(s) 2026. CC BY 4.0 License.

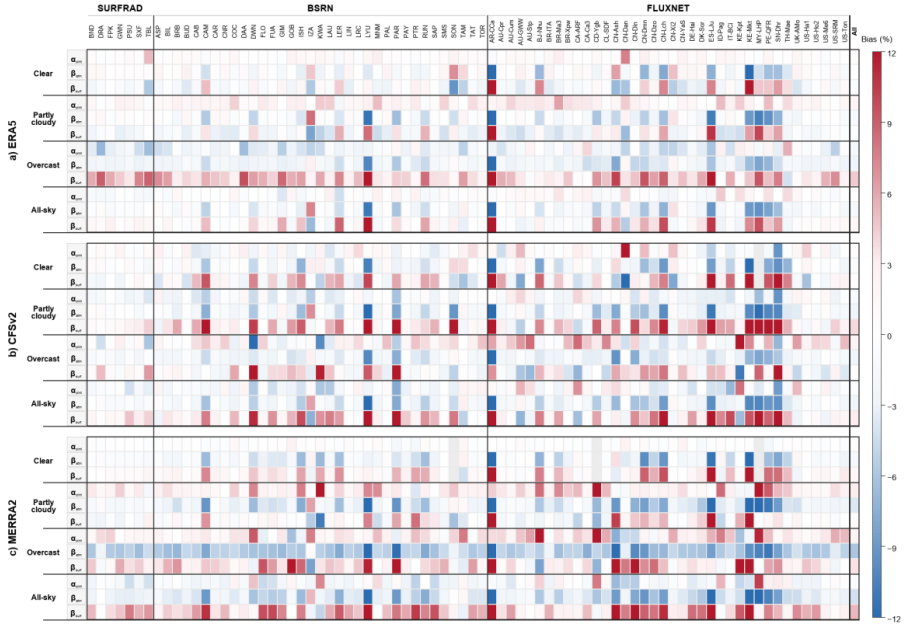


Figure 9. Station-level biases in planetary albedo, atmospheric absorptance, and surface absorptance under clear, partly cloudy, overcast, and all-sky conditions for a) ERA5, b) CFSv2, and c) MERRA2, with stations grouped by SURFRAD, BSRN, and FLUXNET, and the rightmost column showing the overall bias across all stations for each sky condition (α_{plnt}: planetary albedo, β_{atm}: atmospheric absorptance, β_{surf}: surface absorptance).

5. Conclusions

This study comprehensively evaluates the solar energy disposition (SED) of three widely used reanalysis products using collocated satellite and ground observations. The evaluation covers 80 BSRN, SURFRAD, and FLUXNET stations during 2012–2025. The results indicate that ERA5 has the highest overall accuracy and most consistent performance across stations for the three SED variables (planetary albedo, atmospheric absorptance, and surface absorptance). By comparison, CFSv2 SED is marginally superior to MERRA2 SED overall, but its accuracy exhibits notable fluctuations across stations. MERRA2, on the other hand, shows more consistent error directions across stations but exhibits pronounced systematic deviations. Despite their relatively lower SED quality, CFSv2 and MERRA2 still show their respective advantages: CFSv2 performs better for atmospheric absorptance, whereas MERRA2 performs better for planetary albedo and surface absorptance. Furthermore, ERA5 provides the most accurate fractional cloud cover, followed by CFSv2, while MERRA2 yields the poorest performance, with a substantial underestimation of fractional cloud cover. Reanalysis performance also differs among the four aridity classes. Across all three products, planetary albedo and surface absorptance errors are generally larger at humid stations than at arid stations. For atmospheric absorptance, errors tend to be larger in the semi-arid and humid groups than in the arid and sub-humid groups. These results indicate that reanalysis SED

https://doi.org/10.5194/egusphere-2026-5749
Preprint. Discussion started: 19 November 2026
© Author(s) 2026. CC BY 4.0 License.

accuracy varies with background hydroclimatic conditions, most consistently for planetary albedo and surface absorptance.

Our evaluations reveal that current reanalysis products still exhibit two clear shortcomings in representing solar energy disposition within the Earth–atmosphere system. First, systematic deviations are evident in the instantaneous all-sky evaluation and become more pronounced under overcast conditions. Under all-sky conditions, all three reanalyses underestimate atmospheric absorptance and overestimate surface absorptance, while planetary albedo is nearly unbiased in ERA5 but underestimated in CFSv2 and MERRA2. These deviations are most pronounced in MERRA2. Under overcast conditions, the underestimation of atmospheric absorptance increases in all three reanalyses. In ERA5, the resulting negative bias is offset mainly by an overestimation of surface absorptance, whereas in CFSv2 and MERRA2, it is offset by overestimations of both planetary albedo and surface absorptance. Second, reanalyses have limited ability to capture the variability of atmospheric absorptance. Under instantaneous all-sky conditions, the R^2 values are only 0.12–0.14, and the standard deviations from all three reanalyses are less than half of those from observations. This limited representation of variability remains evident in the daily and monthly evaluations based on daylight-hour samples. Thus, reanalyses largely fail to reproduce the natural variability of atmospheric absorptance.

Several limitations of this study should be acknowledged. First, the evaluation is based on observations from 80 stations, but their geographical distribution remains uneven, with relatively sparse coverage in some regions. Second, under partly cloudy conditions, point-specific surface incident radiation measurements may not adequately represent the average conditions over larger reanalysis grids at the instantaneous timescale. Finally, this study does not investigate the underlying causes of the identified reanalysis shortcomings, as such factors are likely complex and beyond the scope of the present work.

Code availability. The analysis code used in this study for solar energy disposition calculations is publicly available on Zenodo at https://doi.org/10.5281/zenodo.18396487 (Fu, 2026).

Data availability. The BSRN observation is provided by the World Radiation Monitoring Center, available at https://bsrn.awi.de. The SURFRAD observation is provided by the NOAA Earth System Research Laboratories, available at https://gml.noaa.gov. FLUXNET observation is provided through the FLUXNET2015 data portal at https://fluxnet.org/data/fluxnet2015-dataset/. The CERES and MODIS products are available at https://ceres.larc.nasa.gov and https://search.earthdata.nasa.gov, respectively. ECMWF ERA5 dataset is provided by the European Centre for Medium-Range Weather Forecasts, available at https://cds.climate.copernicus.eu. NCEP CFSv2 dataset is provided by the National Centers for Environmental Prediction, available at https://rda.ucar.edu/. NASA MERRA2 dataset is provided by the NASA Global Modeling and Assimilation Office, available at https://gmao.gsfc.nasa.gov.

Author contributions. GHH designed the research, with contributions from YJF. YJF performed the calculations. GHH and YJF wrote the paper. PFZ, XDZ, SHZ, XHH, and XFW provided feedback on data and comments on the paper.

Competing interests. The contact author has declared that none of the authors has any competing interests.

https://doi.org/10.5194/egusphere-2026-5749
Preprint. Discussion started: 19 November 2026
© Author(s) 2026. CC BY 4.0 License.



Disclaimer. Publisher's note: Copernicus Publications remains neutral with regard to jurisdictional claims made in the text, published maps, institutional affiliations, or any other geographical representation in this paper. While Copernicus Publications makes every effort to include appropriate place names, the final responsibility lies with the authors. Also, please note that this paper has not received English language copy-editing. Views expressed in the text are those of the authors and do not necessarily reflect the views of the publisher.

Acknowledgements. We thank the BSRN, SURFRAD and FLUXNET communities for providing high-quality surface observations, and the CERES and MODIS science teams for their advanced satellite products. We also thank ECMWF, NCEP, and NASA for providing the ERA5, CFSv2, and MERRA2 datasets, respectively. In particular, the computations were supported by the Supercomputing Center of Lanzhou University.

Financial support. This research is supported by the National Natural Science Foundation of China (42371365) and the Science and Technology Program of Gansu Province (23JRRA1059).

References

American Meteorological Society, 2026: Glossary of Meteorology: https://www.ametsoc.org/ams/publications/glossary-of-meteorology/.

Augustine, J. A., DeLuisi, J. J., and Long, C. N.: SURFRAD–A National Surface Radiation Budget Network for Atmospheric Research, Bulletin of the American Meteorological Society, 81, 2341-2358, https://doi.org/10.1175/1520-0477(2000)081<2341:SANSRB>2.3.CO;2, 2000.

Battisti, D. S. and Donohoe, A.: Atmospheric and Surface Contributions to Planetary Albedo, Journal of Climate, 24, 4402-4418, https://doi.org/10.1175/2011jcli3946.1, 2011.

Fu, Y.-J., Huang, G.-H., Huang, Z.-Y., Wang, X.-F., Ma, H., Wang, G.-J., Huang, C.-L., Hao, X.-H., and Zhao, P.-F.: Is the cloud absorption of solar radiation still underestimated notably by current model-based reanalyses?, Advances in Climate Change Research, 17, 12-24, https://doi.org/10.1016/j.accre.2025.10.003, 2026.

García, R. D., Cuevas, E., Ramos, R., Cachorro, V. E., Redondas, A., and Moreno-Ruiz, J. A.: Description of the Baseline Surface Radiation Network (BSRN) station at the Izaña Observatory (2009–2017): measurements and quality control/assurance procedures, Geoscientific Instrumentation, Methods and Data Systems, 8, 77-96, https://doi.org/10.5194/gi-8-77-2019, 2019.

Gelaro, R., McCarty, W., Suárez, M. J., Todling, R., Molod, A., Takacs, L., Randles, C. A., Darmenov, A., Bosilovich, M. G., Reichle, R., Wargan, K., Coy, L., Cullather, R., Draper, C., Akella, S., Buchard, V., Conaty, A., da Silva, A. M., Gu, W., Kim, G. K., Koster, R., Lucchesi, R., Merkova, D., Nielsen, J. E., Partyka, G., Pawson, S., Putman, W., Rienecker, M., Schubert, S. D., Sienkiewicz, M., and Zhao, B.: The Modern-Era Retrospective Analysis for Research and Applications, Version 2 (MERRA-2), JOURNAL OF CLIMATE, 30, 5419-5454, https://doi.org/10.1175/JCLI-D-16-0758.1, 2017.

Hersbach, H., Bell, B., Berrisford, P., Hirahara, S., Horányi, A., Muñoz-Sabater, J., Nicolas, J., Peubey, C., Radu, R., Schepers, D., Simmons, A., Soci, C., Abdalla, S., Abellan, X., Balsamo, G., Bechtold, P., Biavati, G., Bidlot, J., Bonavita, M., De Chiara, G., Dahlgren, P., Dee, D., Diamantakis, M., Dragani, R., Flemming, J., Forbes, R., Fuentes, M., Geer, A., Haimberger, L., Healy, S., Hogan, R. J., Hólm, E., Janisková, M., Keeley, S., Laloyaux, P., Lopez, P., Lupu, C., Radnoti, G., de Rosnay, P., Rozum, I., Vamborg, F., Villaume, S., and Thépaut, J. N.: The ERA5 global reanalysis, QUARTERLY JOURNAL OF THE ROYAL METEOROLOGICAL SOCIETY, 146, 1999-2049, https://doi.org/10.1002/qj.3803, 2020.

Hobbins, M., Jansma, T., Sarmiento, D. P., McNally, A., Magadzire, T., Jayanthi, H., Turner, W., Hoell, A., Husak, G., Senay, G., Boiko, O., Budde, M., Mogane, P., and Dewes, C. F.: A global long-term daily reanalysis of reference evapotranspiration for drought and food-security monitoring, Sci Data, 10, 746, https://doi.org/10.1038/s41597-023-02648-4, 2023.

https://doi.org/10.5194/egusphere-2026-5749
Preprint. Discussion started: 19 November 2026
© Author(s) 2026. CC BY 4.0 License.

Huang, G., Li, X., Huang, C., Liu, S., Ma, Y., and Chen, H.: Representativeness errors of point-scale ground-based solar radiation measurements in the validation of remote sensing products, Remote Sensing of Environment, 181, 198-206, https://doi.org/10.1016/j.rse.2016.04.001, 2016.

Huang, G., Li, Z., Li, X., Liang, S., Yang, K., Wang, D., and Zhang, Y.: Estimating surface solar irradiance from satellites: Past, present, and future perspectives, Remote Sensing of Environment, 233, https://doi.org/10.1016/j.rse.2019.111371, 2019.

Jiang, H., Lu, N., Huang, G., Yao, L., Qin, J., and Liu, H.: Spatial scale effects on retrieval accuracy of surface solar radiation using satellite data, Applied Energy, 270, https://doi.org/10.1016/j.apenergy.2020.115178, 2020.

Jiao, B., Li, Q., Sun, W., and Martin, W.: Uncertainties in the global and continental surface solar radiation variations: inter-comparison of in-situ observations, reanalyses, and model simulations, Climate Dynamics, 59, 2499-2516, https://doi.org/10.1007/s00382-022-06222-3, 2022.

Li, Z. and Moreau, L.: Alteration of atmospheric solar absorption by clouds: Simulation and observation, Journal of Applied Meteorology and Climatology, 35, 653-670, https://doi.org/10.1175/1520-0450(1996)035<0653:AOASAB>2.0.CO;2, 1996.

Li, Z. and Trishchenko, A. P.: Quantifying uncertainties in determining SW cloud radiative forcing and cloud absorption due to variability in atmospheric conditions, Journal of the atmospheric sciences, 58, 376-389, https://doi.org/10.1175/1520-0469(2001)058<0376:QUIDSC>2.0.CO;2, 2001.

Li, Z., Moreau, L., and Arking, A.: On solar energy disposition: A perspective from observation and modeling, Bulletin of the American Meteorological Society, 78, 53-70, https://doi.org/10.1175/1520-0477(1997)078<0053:OSEDAP>2.0.CO;2, 1997.

Loeb, N. G., Doelling, D. R., Wang, H., Su, W., Nguyen, C., Corbett, J. G., Liang, L., Mitrescu, C., Rose, F. G., and Kato, S.: Clouds and the Earth's Radiant Energy System (CERES) Energy Balanced and Filled (EBAF) Top-of-Atmosphere (TOA) Edition-4.0 Data Product, Journal of Climate, 31, 895-918, https://doi.org/10.1175/jcli-d-17-0208.1, 2018.

Minnis, P., Sun-Mack, S., Chen, Y., Chang, F.-L., Yost, C. R., Smith, W. L., Heck, P. W., Arduini, R. F., Bedka, S. T., Yi, Y., Hong, G., Jin, Z., Painemal, D., Palikonda, R., Scarino, B. R., Spangenberg, D. A., Smith, R. A., Trepte, Q. Z., Yang, P., and Xie, Y.: CERES MODIS Cloud Product Retrievals for Edition 4—Part I: Algorithm Changes, IEEE Transactions on Geoscience and Remote Sensing, 59, 2744-2780, https://doi.org/10.1109/tgrs.2020.3008866, 2021.

Norris, J. R., Allen, R. J., Evan, A. T., Zelinka, M. D., O'Dell, C. W., and Klein, S. A.: Evidence for climate change in the satellite cloud record, Nature, 536, 72-75, https://doi.org/10.1038/nature18273, 2016.

Pastorello, G., Trotta, C., Canfora, E., Chu, H., Christianson, D., Cheah, Y. W., Poindexter, C., Chen, J., Elbashandy, A., Humphrey, M., Isaac, P., Polidori, D., Reichstein, M., Ribeca, A., van Ingen, C., Vuichard, N., Zhang, L., Amiro, B., Ammann, C., Arain, M. A., Ardo, J., Arkebauer, T., Arndt, S. K., Arriga, N., Aubinet, M., Aurela, M., Baldocchi, D., Barr, A., Beamesderfer, E., Marchesini, L. B., Bergeron, O., Beringer, J., Bernhofer, C., Berveiller, D., Billesbach, D., Black, T. A., Blanken, P. D., Bohrer, G., Boike, J., Bolstad, P. V., Bonal, D., Bonnefond, J. M., Bowling, D. R., Bracho, R., Brodeur, J., Brummer, C., Buchmann, N., Burban, B., Burns, S. P., Buysse, P., Cale, P., Cavagna, M., Cellier, P., Chen, S., Chini, I., Christensen, T. R., Cleverly, J., Collalti, A., Consalvo, C., Cook, B. D., Cook, D., Coursolle, C., Cremonese, E., Curtis, P. S., D'Andrea, E., da Rocha, H., Dai, X., Davis, K. J., Cinti, B., Grandcourt, A., Ligne, A., De Oliveira, R. C., Delpierre, N., Desai, A. R., Di Bella, C. M., Tommasi, P. D., Dolman, H., Domingo, F., Dong, G., Dore, S., Duce, P., Dufrene, E., Dunn, A., Dusek, J., Eamus, D., Eichelmann, U., ElKhidir, H. A. M., Eugster, W., Ewenz, C. M., Ewers, B., Famulari, D., Fares, S., Feigenwinter, I., Feitz, A., Fensholt, R., Filippa, G., Fischer, M., Frank, J., Galvagno, M., Gharun, M., Gianelle, D., Gielen, B., Gioli, B., Gitelson, A., Goded, I., Goeckede, M., Goldstein, A. H., Gough, C. M., Goulden, M. L., Graf, A., Griebel, A., Gruening, C., Grunwald, T., Hammerle, A., Han, S., Han, X., Hansen, B. U., Hanson, C., Hatakka, J., He, Y., Hehn, M., Heinesch, B., Hinko-Najera, N., Hortnagl, L., Hutley, L., Ibrom, A., Ikawa, H., Jackowicz-Korczynski, M., Janous, D., Jans, W., Jassal, R., Jiang, S., Kato, T., Khomik, M., Klatt, J., Knohl, A., Knox, S., Kobayashi, H., Koerber, G., Kolle, O., Kosugi, Y., Kotani, A., Kowalski, A., Kruijt, B., Kurbatova, J., Kutsch, W. L., Kwon, H., Launiainen, S., Laurila, T., Law, B., Leuning, R., Li, Y., Liddell, M., Limousin, J. M., Lion, M., Liska, A. J., Lohila, A., Lopez-Ballesteros, A., Lopez-Blanco, E., Loubet, B., Loustau, D., Lucas-Moffat, A., Luers, J., Ma, S., Macfarlane, C., Magliulo, V., Maier, R., Mammarella, I., Manca, G., Marcolla, B., Margolis, H. A., Marras, S., Massman, W., Mastepanov, M., Matamala, R., Matthes, J. H., Mazzenga, F., McCaughey, H., McHugh, I., McMillan, A. M. S., Merbold, L., Meyer, W., Meyers, T., Miller, S. D., Minerbi, S., Moderow, U., Monson, R. K., Montagnani, L., Moore, C. E., Moors, E., Moreaux, V., Moureaux, C., Munger, J. W., Nakai, T., Neirynck, J., Nesic, Z., Nicolini, G., Noormets, A., Northwood, M., Nosetto, M., Nouvellon, Y., Novick, K., Oechel, W., Olesen, J. E., Ourcival, J. M., Papuga, S. A., Parmentier, F.

https://doi.org/10.5194/egusphere-2026-5749
Preprint. Discussion started: 19 November 2026
© Author(s) 2026. CC BY 4.0 License.

J., Paul-Limoges, E., Pavelka, M., Peichl, M., Pendall, E., Phillips, R. P., Pilegaard, K., Pirk, N., Posse, G., Powell, T., Prasse, H., Prober, S. M., Rambal, S., Rannik, U., Raz-Yaseef, N., Rebmann, C., Reed, D., Dios, V. R., Restrepo-Coupe, N., Reverter, B. R., Roland, M., Sabbatini, S., Sachs, T., Saleska, S. R., Sanchez-Canete, E. P., Sanchez-Mejia, Z. M., Schmid, H. P., Schmidt, M., Schneider, K., Schrader, F., Schroder, I., Scott, R. L., Sedlak, P., Serrano-Ortiz, P., Shao, C., Shi, P., Shironya, I., Siebicke, L., Sigut, L., Silberstein, R., Sirca, C., Spano, D., Steinbrecher, R., Stevens, R. M., Sturtevant, C., Suyker, A., Tagesson, T., Takanashi, S., Tang, Y., Tapper, N., Thom, J., Tomassucci, M., Tuovinen, J. P., Urbanski, S., Valentini, R., van der Molen, M., van Gorsel, E., van Huissteden, K., Varlagin, A., Verfaillie, J., Vesala, T., Vincke, C., Vitale, D., Vygodskaya, N., Walker, J. P., Walter-Shea, E., Wang, H., Weber, R., Westermann, S., Wille, C., Wofsy, S., Wohlfahrt, G., Wolf, S., Woodgate, W., Li, Y., Zampedri, R., Zhang, J., Zhou, G., Zona, D., Agarwal, D., Biraud, S., Torn, M., and Papale, D.: The FLUXNET2015 dataset and the ONEFlux processing pipeline for eddy covariance data, Sci Data, 7, 225, https://doi.org/10.1038/s41597-020-0534-3, 2020.

Saha, S., Moorthi, S., Wu, X., Wang, J., Nadiga, S., Tripp, P., Behringer, D., Hou, Y.-T., Chuang, H.-y., and Iredell, M.: The NCEP climate forecast system version 2, Journal of climate, 27, 2185-2208, https://doi.org/10.1175/JCLI-D-12-00823.1, 2014.

Trenberth, K. E., Fasullo, J. T., O'Dell, C., and Wong, T.: Relationships between tropical sea surface temperature and top-of-atmosphere radiation, Geophysical Research Letters, 37, https://doi.org/10.1029/2009gl042314, 2010.

Trenberth, K. E., Zhang, Y., Fasullo, J. T., and Taguchi, S.: Climate variability and relationships between top-of-atmosphere radiation and temperatures on Earth, Journal of Geophysical Research: Atmospheres, 120, 3642-3659, https://doi.org/10.1002/2014jd022887, 2015.

Wang, Y., He, Z., Zhao, W., Yin, G., Guan, X., and Xie, X.: A global hourly gross primary production dataset from 2001 to 2020, Scientific Data, 13, https://doi.org/10.1038/s41597-025-06371-0, 2025.

Wild, M. and Bosilovich, M. G.: The Global Energy Balance as Represented in Atmospheric Reanalyses, Surveys in Geophysics, 45, 1799-1825, https://doi.org/10.1007/s10712-024-09861-9, 2024.

Yang, S., Zhang, X., Guan, S., Zhao, W., Duan, Y., Yao, Y., Jia, K., and Jiang, B.: A review and comparison of surface incident shortwave radiation from multiple data sources: satellite retrievals, reanalysis data and GCM simulations, International Journal of Digital Earth, 16, 1332-1357, https://doi.org/10.1080/17538947.2023.2198262, 2023.

Zhang, X., Lu, N., Jiang, H., and Yao, L.: Evaluation of Reanalysis Surface Incident Solar Radiation Data in China, Sci Rep, 10, 3494, https://doi.org/10.1038/s41598-020-60460-1, 2020.

Zhang, X., Liang, S., Wang, G., Yao, Y., Jiang, B., and Cheng, J.: Evaluation of the Reanalysis Surface Incident Shortwave Radiation Products from NCEP, ECMWF, GSFC, and JMA Using Satellite and Surface Observations, Remote Sensing, 8, https://doi.org/10.3390/rs8030225, 2016.

Zomer, R. J., Xu, J., and Trabucco, A.: Version 3 of the Global Aridity Index and Potential Evapotranspiration Database, Sci Data, 9, 409, https://doi.org/10.1038/s41597-022-01493-1, 2022.

APPENDIX

Appendix A. Basic information of stations

Table A1. Basic information of the BSRN, SURFRAD and FLUXNET stations

Site ID	Station name	Latitude	Longitude	Elevation (m)	Network	Surface type
ASP	Alice Springs	−23.79800	133.88800	547.0	BSRN	Grass
BIL	Billings	36.60500	−97.51600	317.0	BSRN	Grass
BRB	Brasilia	−15.60100	−47.71300	1023.0	BSRN	Concrete (shrub since 2015)
BUD	Budapest-Lorinc	47.42910	19.18220	139.1	BSRN	Grass
CAB	Cabauw	51.97110	4.92670	0.0	BSRN	Grass
CAM	Camborne	50.21670	−5.31670	88.0	BSRN	Grass
CAR	Carpentras	44.08300	5.05900	100.0	BSRN	Cultivated
CNR	Cener	42.81600	−1.60100	471.0	BSRN	Asphalt
COC	Cocos Island	−12.19300	96.83500	0.0	BSRN	Grass
DAA	De Aar	−30.66670	23.99300	1287.0	BSRN	Sand
DWN	Darwin Met Office	−12.42400	130.89250	32.0	BSRN	Grass

https://doi.org/10.5194/egusphere-2026-5749
Preprint. Discussion started: 19 November 2026
© Author(s) 2026. CC BY 4.0 License.

FLO	Florianopolis	−27.60470	−48.52270	11.0	BSRN	Concrete
FUA	Fukuoka	33.58220	130.37640	3.0	BSRN	Asphalt
GIM	Granite Island	46.72100	−87.41100	208.0	BSRN	Grass
GOB	Gobabeb	−23.56140	15.04200	407.0	BSRN	Desert gravel
ISH	Ishigakijima	24.33670	124.16440	6.0	BSRN	Asphalt
IZA	Izaña	28.30930	−16.49930	2373.0	BSRN	Rock
KWA	Kwajalein	8.72000	167.73100	10.0	BSRN	Water (ocean)
LAU	Lauder	−45.04500	169.68900	350.0	BSRN	Grass
LER	Lerwick	60.13890	−1.18470	80.0	BSRN	Grass
LIN	Lindenberg	52.21000	14.12200	125.0	BSRN	Cultivated
LRC	Langley Research Center	37.10380	−76.38720	3.0	BSRN	Grass
LYU	Lanyu Station	22.03700	121.55830	324.0	BSRN	Mixed forest
MNM	Minamitorishima	24.28830	153.98330	7.0	BSRN	Water (ocean)
PAL	Palaiseau, SIRTA Observatory	48.71300	2.20800	156.0	BSRN	Concrete
PAR	Paramaribo	5.80600	−55.21460	4.0	BSRN	Grass
PAY	Payerne	46.81500	6.94400	491.0	BSRN	Cultivated
PTR	Petrolina	−9.06800	−40.31900	387.0	BSRN	Concrete (shrub since 2015)
RUN	Reunion Island, University	−20.90140	55.48360	116.0	BSRN	Concrete
SAP	Sapporo	43.06000	141.32860	17.0	BSRN	Asphalt
SMS	São Martinho da Serra	−29.44280	−53.82310	489.0	BSRN	Concrete (grass since 2015)
SON	Sonnblick	47.05400	12.95770	3109.0	BSRN	Rock
TAM	Tamanrasset	22.79030	5.52920	1385.0	BSRN	Desert rock
TAT	Tateno	36.05810	140.12580	25.0	BSRN	Grass
TOR	Toravere	58.25400	26.46200	70.0	BSRN	Grass
BND	Bondville, Illinois	40.05192	−88.37309	213.0	SURFRAD	Grass
DRA	Desert Rock, Nevada	36.62373	−116.01947	1007.0	SURFRAD	Desert gravel
FPK	Fort Peck, Montana	48.30783	−105.10170	634.0	SURFRAD	Grass
GWN	Goodwin Creek, Mississippi	34.25470	−89.87290	98.0	SURFRAD	Grass
PSU	Penn. State Univ., Pennsylvania	40.72012	−77.93085	376.0	SURFRAD	Cultivated
SXF	Sioux Falls, South Dakota	43.73403	−96.62328	473.0	SURFRAD	Grass
TBL	Table Mountain, Boulder, Colorado	40.12498	−105.23680	1689.0	SURFRAD	Grass
AR-CCa	Carlos Casares agriculture	−35.62100	−61.31810	83.0	FLUXNET	Croplands
AU-Cpr	Calperum Chowilla	−34.00270	140.58770	60	FLUXNET	Savannas
AU-Cum	Cumberland Plain	−33.61528	150.72361	35	FLUXNET	Cropland/Natural Vegetation Mosaics
AU-GWW	Great Western Woodlands	−30.19140	120.65417	444	FLUXNET	Closed Shrublands
AU-Stp	Sturt Plains	−17.15070	133.35020	227	FLUXNET	Grasslands
BJ-Nhu	Nalohou	9.74000	1.60000	449.0	FLUXNET	Savannas
BR-ITA	MataFLUX: Multi-species tree restoration planting	−23.06040	−48.64670	820.0	FLUXNET	Evergreen Broadleaf Forests
BR-Ma3	ZF3, Colosso farm	−2.39070	−59.88350	147.0	FLUXNET	Cropland/Natural Vegetation Mosaics
BR-Xpw	XomanoFlux	−16.37300	−56.46100	124.0	FLUXNET	Grasslands

https://doi.org/10.5194/egusphere-2026-5749
Preprint. Discussion started: 19 November 2026
© Author(s) 2026. CC BY 4.0 License.

CA-ARF	Attawapiskat River Fen	52.70080	−83.95500	88.0	FLUXNET	Permanent Wetlands
CA-Ca3	British Columbia - Pole sapling Douglas-fir stand	49.53460	−124.90040	170	FLUXNET	Evergreen Needleleaf Forests
CD-Ygb	Yangambi	0.81444	24.50247	466.0	FLUXNET	Mixed Forests
CL-SDF	Senda Darwin Forest	−41.88300	−73.67600	50.0	FLUXNET	Evergreen Broadleaf Forests
CN-Ash	Ailaoshan	24.53806	101.02917	2551	FLUXNET	Evergreen Broadleaf Forests
CN-Dan	Dangxiong	30.49780	91.06640	4315	FLUXNET	Grasslands
CN-Din	Dinghushan	23.17330	112.53610	295	FLUXNET	Evergreen Broadleaf Forests
CN-Dmn	Daman	38.85551	100.37223	1556.0	FLUXNET	Croplands
CN-Dzo	Danzhou	19.54600	109.47500	151	FLUXNET	Evergreen Broadleaf Forests
CN-Lch	Luancheng	37.88936	114.69289	50	FLUXNET	Croplands
CN-Xi2	Xilinhot grassland site (X03)	43.55444	116.67140	1256	FLUXNET	Grasslands
CN-YaS	Yanchi natural shrubland	37.70877	107.22655	1521	FLUXNET	Open Shrublands
DE-Hai	Hainich	51.07921	10.45217	438.7	FLUXNET	Deciduous Broadleaf Forests
DK-Sor	Soroe	55.48587	11.64464	55.0	FLUXNET	Deciduous Broadleaf Forests
ES-LJu	Llano de los Juanes	36.92659	−2.75212	1600.0	FLUXNET	Open Shrublands
ID-Pag	Palangkaraya undrained forest	−2.32392	113.90439	22.0	FLUXNET	Evergreen Broadleaf Forests
IT-BCi	Borgo Cioffi	40.52375	14.95744	10.0	FLUXNET	Croplands
KE-Kpt	Kapiti	−1.61419	37.13311	1671	FLUXNET	Grasslands
KE-Mkt	Maktau	−3.42586	38.14066	1074.6	FLUXNET	Croplands
MY-LHP	Lambir Hills National Park	4.20101	114.03908	200.0	FLUXNET	Evergreen Broadleaf Forests
PE-QFR	Quistococha Forest Reserve	−3.83440	−73.31900	104.0	FLUXNET	Permanent Wetlands
SN-Dhr	Dahra	15.40256	−15.43214	50.0	FLUXNET	Grasslands
TH-Mae	Mae Moh plantation	18.42264	99.72025	380.0	FLUXNET	Deciduous Broadleaf Forests
UK-AMo	Auchencorth Moss	55.79255	−3.24369	268.0	FLUXNET	Permanent Wetlands
US-Ha1	Harvard Forest EMS Tower (HFR1)	42.53780	−72.17150	340.0	FLUXNET	Deciduous Broadleaf Forests
US-Ho2	Howland Forest (west tower)	45.20910	−68.74700	61.0	FLUXNET	Evergreen Needleleaf Forests
US-Me6	Metolius Young Pine Burn	44.32330	−121.60780	998.0	FLUXNET	Evergreen Needleleaf Forests
US-SRM	Santa Rita Mesquite	31.82140	−110.86610	1120.0	FLUXNET	Woody Savannas
US-Ton	Tonzi Ranch	38.43090	−120.96600	177.0	FLUXNET	Woody Savannas

Appendix B. Daily and monthly SED evaluation

The supporting daily and monthly evaluations use hourly CERES SYN1deg TOA fluxes on a 1° grid. Ground-based shortwave measurements are averaged to hourly intervals. MODIS MCD43A3 albedo and the ERA5, CFSv2, and MERRA2 fields are aggregated to the same 1° grid before data matching. The

https://doi.org/10.5194/egusphere-2026-5749
Preprint. Discussion started: 19 November 2026
© Author(s) 2026. CC BY 4.0 License.

three SED components are calculated for valid matched daylight hours and then averaged to daily means. Monthly means are calculated from the valid daily means within each month. Summary statistics are listed in Tables B1–B3.

The daily and monthly evaluations are generally consistent with the instantaneous results. ERA5 continues to show the smallest overall errors, while CFSv2 and MERRA2 underestimate planetary albedo and atmospheric absorptance and overestimate surface absorptance. Monthly averaging reduces the RMSEs of all three components relative to the daily scale. At the monthly scale, the overall R^2 values range from 0.74 to 0.90 for planetary albedo and from 0.66 to 0.78 for surface absorptance, but remain only 0.21–0.30 for atmospheric absorptance. The daily results retain the aridity-related contrast in planetary albedo and surface absorptance, with lower RMSEs at arid than at humid stations for all three reanalyses. This contrast is weaker after monthly averaging, particularly for CFSv2. Atmospheric absorptance remains non-monotonic across the four aridity classes at both time scales.

Table B1. Statistics of ECMWF ERA5 for the three SED components across all stations and the four aridity classes at daily and monthly scales under all-sky conditions.

Time scale	Aridity class	Variables	Obs. mean (%)	Bias (%)	MAE (%)	RMSE (%)	Relative RMSE (%)	R^2
Daily	All	Planetary albedo	30.36	−0.20	4.56	6.39	21.04	0.79
		Atmospheric absorptance	24.41	−0.98	4.77	6.78	27.77	0.18
		Surface absorptance	45.23	1.17	6.51	8.92	19.73	0.72
	Arid	Planetary albedo	26.11	−0.17	3.08	4.57	17.50	0.71
		Atmospheric absorptance	22.01	−0.25	3.35	4.87	22.14	0.37
		Surface absorptance	51.88	0.42	4.60	6.59	12.71	0.69
	Semi-arid	Planetary albedo	25.68	−0.18	3.93	5.66	22.03	0.74
		Atmospheric absorptance	22.75	−0.71	5.57	7.99	35.14	0.13
		Surface absorptance	51.57	0.89	6.92	9.50	18.42	0.61
	Sub-humid	Planetary albedo	29.16	−0.13	4.63	6.41	21.97	0.78
		Atmospheric absorptance	23.06	0.20	3.74	5.07	21.98	0.18
		Surface absorptance	47.78	−0.07	5.81	7.79	16.30	0.76
	Humid	Planetary albedo	32.99	−0.22	5.10	6.95	21.06	0.78
		Atmospheric absorptance	25.70	−1.42	5.03	7.00	27.23	0.12
		Surface absorptance	41.32	1.63	6.95	9.39	22.72	0.72
Monthly	All	Planetary albedo	30.46	−0.22	2.00	2.63	8.63	0.90
		Atmospheric absorptance	24.34	−0.93	2.68	4.30	17.69	0.26
		Surface absorptance	45.20	1.16	3.37	4.91	10.87	0.78
	Arid	Planetary albedo	26.12	−0.18	1.66	2.07	7.91	0.75
		Atmospheric absorptance	22.01	−0.25	2.00	3.33	15.15	0.43
		Surface absorptance	51.86	0.42	2.68	3.92	7.56	0.66
	Semi-arid	Planetary albedo	25.65	−0.19	1.97	2.81	10.94	0.82
		Atmospheric absorptance	22.53	−0.52	3.89	5.74	25.49	0.17
		Surface absorptance	51.82	0.72	4.39	6.11	11.79	0.62
	Sub-humid	Planetary albedo	29.38	−0.18	2.03	2.68	9.13	0.87
		Atmospheric absorptance	23.01	0.20	1.47	1.96	8.50	0.29
		Surface absorptance	47.61	−0.02	2.44	3.14	6.60	0.84
	Humid	Planetary albedo	33.12	−0.25	2.09	2.68	8.09	0.90
		Atmospheric absorptance	25.64	−1.39	2.65	4.24	16.55	0.13
		Surface absorptance	41.24	1.64	3.36	4.93	11.95	0.75

Table B2. Statistics of NCEP CFSv2 for the three SED components across all stations and the four aridity classes at daily and monthly scales under all-sky conditions.

https://doi.org/10.5194/egusphere-2026-5749
Preprint. Discussion started: 19 November 2026
© Author(s) 2026. CC BY 4.0 License.

Time scale	Aridity class	Variables	Obs. mean (%)	Bias (%)	MAE (%)	RMSE (%)	Relative RMSE (%)	R^2
Daily	All	Planetary albedo	30.35	−0.76	7.00	9.74	32.10	0.62
		Atmospheric absorptance	24.41	−1.70	4.88	7.00	28.68	0.16
		Surface absorptance	45.24	2.46	8.73	12.01	26.55	0.58
	Arid	Planetary albedo	26.10	−0.46	5.65	7.93	30.37	0.40
		Atmospheric absorptance	22.01	−1.04	3.58	5.27	23.96	0.26
		Surface absorptance	51.89	1.50	7.48	10.32	19.89	0.37
	Semi-arid	Planetary albedo	25.67	−0.10	5.83	8.53	33.24	0.56
		Atmospheric absorptance	22.75	−1.65	5.52	8.03	35.32	0.16
		Surface absorptance	51.58	1.75	8.38	11.95	23.17	0.47
	Sub-humid	Planetary albedo	29.15	−1.71	6.63	9.38	32.18	0.62
		Atmospheric absorptance	23.06	−0.49	3.67	5.03	21.81	0.20
		Surface absorptance	47.79	2.20	7.36	10.41	21.77	0.63
	Humid	Planetary albedo	32.97	−0.89	7.73	10.51	31.87	0.63
		Atmospheric absorptance	25.70	−2.06	5.19	7.29	28.35	0.09
		Surface absorptance	41.33	2.95	9.35	12.62	30.54	0.59
Monthly	All	Planetary albedo	30.45	−0.75	3.36	4.36	14.31	0.79
		Atmospheric absorptance	24.34	−1.64	2.95	4.63	19.01	0.21
		Surface absorptance	45.21	2.39	4.98	6.77	14.98	0.66
	Arid	Planetary albedo	26.11	−0.45	3.57	4.66	17.85	0.21
		Atmospheric absorptance	22.01	−1.03	2.35	3.90	17.74	0.24
		Surface absorptance	51.87	1.48	5.19	7.36	14.19	0.11
	Semi-arid	Planetary albedo	25.64	−0.11	2.98	3.99	15.57	0.70
		Atmospheric absorptance	22.52	−1.47	3.88	5.73	25.46	0.24
		Surface absorptance	51.84	1.57	5.39	7.33	14.14	0.50
	Sub-humid	Planetary albedo	29.38	−1.74	3.12	4.02	13.69	0.80
		Atmospheric absorptance	23.01	−0.47	1.56	1.95	8.48	0.32
		Surface absorptance	47.61	2.21	3.53	4.47	9.38	0.79
	Humid	Planetary albedo	33.12	−0.86	3.46	4.44	13.41	0.81
		Atmospheric absorptance	25.64	−2.02	3.01	4.68	18.27	0.05
		Surface absorptance	41.24	2.88	5.02	6.73	16.33	0.68

Table B3. Statistics of NASA MERRA2 for the three SED components across all stations and the four aridity classes at daily and monthly scales under all-sky conditions.

Time scale	Aridity class	Variables	Obs. mean (%)	Bias (%)	MAE (%)	RMSE (%)	Relative RMSE (%)	R^2
Daily	All	Planetary albedo	30.34	−0.56	6.05	8.71	28.71	0.62
		Atmospheric absorptance	24.41	−3.58	5.41	7.61	31.19	0.19
		Surface absorptance	45.25	4.13	8.22	11.52	25.45	0.60
	Arid	Planetary albedo	26.09	0.15	3.44	5.52	21.17	0.60
		Atmospheric absorptance	22.01	−2.54	3.62	5.47	24.84	0.38
		Surface absorptance	51.90	2.39	4.90	7.50	14.45	0.64
	Semi-arid	Planetary albedo	25.67	−0.75	4.83	7.06	27.48	0.63
		Atmospheric absorptance	22.75	−2.99	5.92	8.42	37.01	0.16
		Surface absorptance	51.58	3.74	7.89	11.08	21.48	0.53
	Sub-humid	Planetary albedo	29.14	−0.61	5.98	8.62	29.59	0.61
		Atmospheric absorptance	23.06	−2.35	4.19	5.63	24.41	0.17
		Surface absorptance	47.80	2.95	7.39	10.52	22.00	0.60
	Humid	Planetary albedo	32.96	−0.66	7.07	9.75	29.57	0.60
		Atmospheric absorptance	25.70	−4.19	5.88	8.05	31.34	0.12
		Surface absorptance	41.33	4.86	9.26	12.55	30.36	0.56
Monthly	All	Planetary albedo	30.45	−0.55	3.14	4.39	14.41	0.74
		Atmospheric absorptance	24.34	−3.53	3.99	5.45	22.40	0.30
		Surface absorptance	45.22	4.08	5.27	7.05	15.58	0.68
	Arid	Planetary albedo	26.11	0.14	1.63	2.32	8.90	0.72

https://doi.org/10.5194/egusphere-2026-5749
Preprint. Discussion started: 19 November 2026
© Author(s) 2026. CC BY 4.0 License.

		Atmospheric absorptance	22.01	−2.55	2.72	4.17	18.93	0.47
		Surface absorptance	51.88	2.42	2.87	4.19	8.08	0.74
	Semi-arid	Planetary albedo	25.64	−0.81	2.44	3.39	13.23	0.76
		Atmospheric absorptance	22.52	−2.79	4.64	6.25	27.76	0.22
		Surface absorptance	51.84	3.61	5.44	7.35	14.17	0.58
	Sub-humid	Planetary albedo	29.36	−0.64	3.04	4.18	14.23	0.69
		Atmospheric absorptance	23.01	−2.33	2.56	2.97	12.90	0.36
		Surface absorptance	47.63	2.97	4.42	5.50	11.55	0.64
	Humid	Planetary albedo	33.11	−0.62	3.72	5.02	15.15	0.68
		Atmospheric absorptance	25.64	−4.16	4.31	5.73	22.35	0.17
		Surface absorptance	41.25	4.78	5.91	7.66	18.58	0.60

627